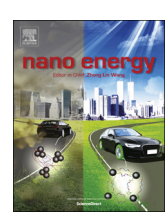
#### Contents lists available at ScienceDirect

## Nano Energy

journal homepage: www.elsevier.com/locate/nanoen



#### Full paper

# Facile and scalable electrodeposition of copper current collectors for highperformance Li-metal batteries



Xuetian Ma, Zhantao Liu, Hailong Chen\*

The Woodruff School of Mechanical Engineering, Georgia Institute of Technology, Atlanta, GA 30332, USA

#### ARTICLE INFO

# Keywords: Lithium-metal batteries Electrodeposition 3-D copper current collector Solid-state batteries

#### ABSTRACT

Lithium metal is a promising anode for high-energy-density batteries owing to its large theoretical capacity and highly negative electrochemical potential. However, its commercial application is stalled by the undesired dendritic growth of lithium during cycling. Here we report a facile one-step electrodeposition process for low-cost, scalable fabrication of copper current collectors with 3-D architected porous structures composed of interconnected nanoparticles of Cu. Li anode deposited onto this porous current collector exhibits good cycling stability of > 340 h in symmetric cells without short-circuit. When tested in full cells with liquid or solid-state electrolyte, the Li anode hosted on the 3-D Cu current collector demonstrates excellent cycling performance with no dendrites formation. This process is extremely simple and scalable for mass production of dendrite-free and high capacity current collector for Li-batteries, which can be easily incorporated into the roll-to-roll manufacturing processes of battery industries.

#### 1. Introduction

With the growing needs for rechargeable batteries with ultrahigh energy densities for portable electronics, electric vehicles, and electrical grids, research efforts beyond conventional Li-ion batteries, such as Li-S [1], Li-O<sub>2</sub>[2], and solid-state batteries [3,4] have been thriving in the last decade. Among the approaches, Li-metal batteries attract a lot of attention, where Li-metal is used as the anode while the cathodes of Li-ion batteries are still used [5,6]. This approach adapts the mature cathode technology from Li-ion batteries and focuses on solving the problems in Li-metal anode, e.g., the dendrite growth and low cyclability [7–9]. This approach not only has the potential for very high energy density, benefiting from the high capacity of Li-metal anode (3840 mAh g $^{-1}$ ), but also has the advantage that it does not need to address the problems in cathode side as Li-S or Li-O<sub>2</sub> batteries do.

The problems of Li-anode are, however, very challenging. Besides the well-known safety problem [10], stripping of Li from the root of the dendrites also results in electrical isolation of some small Li metal pieces (i.e., the "dead Li"[11]) and thus low Coulombic efficiency. A widely accepted model for Li dendrite growth is the space charge model [12]. When the local current density J at the anode exceeds the diffusion-limited value  $J^*$ , limitation in mass transport results in depletion of ions near the surface of the electrode, creating a space charge layer and a strong local electric field, which accelerates a local

deposition or dendritic growth of Li. The space charge theory, however, cannot explain the occasional dendrite growth in low current below  $J^*$ . Another model [13] indicates dendrites can also grow at nucleation sites where local resistivity is low, i.e. areas with good SEI or defects. Tremendous efforts have been made to address the challenges regarding suppression of Li dendrite and stabilization of SEI, including 1) electrolyte engineering [14-18]; 2) interfacial engineering [19-26], [41-44]; 3) use of solid electrolyte [27-29], and 4) use 3-D structured current collectors [30-40]. Among these promising approaches, interfacial engineering and the use of 3-D current collector represent some new promises. Compared to flat foil current collectors, 3-D structured current collectors have much larger active surfaces area, thus effectively reduce the actual current density *J* for the same apparent current and lower the possibility of stimulating dendritic growth. Many 3-D structures of current collectors have been demonstrated to have positive effects to mitigate Li dendrite growth, such as 3D submicron Copper (Cu) skeleton [30], free-standing Cu nanowires (NWs) [31], hollow carbon fibers [32], graphitized carbon fibers [33], de-alloyed 3D porous Cu [34], vertically aligned Cu microchannels [35], crumbled graphene balls [36], pie-like porous Cu NW/graphene [37], carbon fiber papers [38], nitrogen doped graphene [39], and nitrogen doped graphitic carbon foams [40]. Interfacial modification is usually realized by introducing heterogeneous nucleation sites by coating conductive materials (e.g., hollow carbon spheres with nanoparticles seeds inside [41],

E-mail address: hailong.chen@me.gatech.edu (H. Chen).

<sup>\*</sup> Corresponding author.

Li-rich composite alloy films [42]) or insulating layers (e.g., glass fiber cloth [43], poly(dimethylsiloxane) [44]) to facilitate the simultaneous plating of Li on the modified surface.

These works demonstrated the promise of the 3-D structured current collectors and strategies of increasing nucleation sites. However, most of these successes are in lab-scale with coin cells and most of the methods are sophisticated and expensive, not scalable and compatible with the roll-to-roll manufacturing processes of current Li-ion battery industry. For example, the synthesis of Cu nanowires or nanoparticles requires multi-step wet chemistry reaction and following heat treatment [31]. The carbonaceous current collectors, although having excellent performance, do not have high enough mechanical strength to be used as the current collectors for roll-to-roll processing, and it is difficult to bind the carbon films tightly onto any metal foils. Facile, scalable and low-cost method to obtain effective 3-D structured current collector is a challenge yet to be met. Towards addressing this challenge, we report a facile and scalable one-step electrodeposition method to obtain Cu current collector with 3-D surface structures at room temperature. This electrodeposited Cu current collector enabled stable Li plating/stripping for more than 340 h tests under a large current density of 2 mA cm<sup>-2</sup> with a reasonably small voltage hysteresis of less than 50 mV, as well as excellent cycling performance of full cells with LiFePO<sub>4</sub> cathode with liquid electrolyte and TiS<sub>2</sub> cathode in all-solidstate cells. Besides the promising electrochemical performances, this new method distinguishes itself from previous methods in that it is very easy to scale up with no expensive equipment or processing steps required. Electrodeposition of Cu has been widely used for more than a hundred years in many applications and large size electrodeposited Cu foils for pouch cells can be easily produced with low cost. More attractively, the manufacturing of Li-metal cells with using this current collector is not different from the existing Li-ion battery manufacture, which further reduces the barrier to the commercialization of this new technique.

#### 2. Experimental section

#### 2.1. Preparation of electrodeposited Cu film

A typical electrodeposition processing of copper current collector is as follows: A two-electrode system was used and a constant voltage electrodeposition process was controlled with using a battery cycler (Arbin, BT2043). Copper foil with thickness of 0.0005 in. (MTI corp.) and area of about 6.75 cm2 was used as the working electrode, while a platinum plate with area of 0.25 cm<sup>2</sup> was used as the counter electrode. The electrolyte consists of 0.5 M copper sulfate heptahydrate (VWR International LLC) in 20 mL deionized water. In addition, poly(acrylic acid) - 5000 (PAA-5000, 50 wt%, ACROS Organics) and sulfuric acid (95-98%, BDH Chemicals) were used as additives to control the morphology of the deposited Cu surface layer. With using 0.5 mM PAA-5000 and 0.1 M sulfate acid as additives, nanometer-sized clusters can be obtained. The electrodeposition was conducted with potentiostatic mode, with a constant potential of 2.5 V for 20 min. The current density of working electrode was controlled between 3.5 and 3.7 mA cm<sup>-2</sup>, to ensure no Cu dendrite is formed [45]. The reactions at the working electrode and counter electrode are (1) and (2) below, respectively.

$$Cu^{2+} + 2e \rightarrow Cu \tag{1}$$

$$2H_2O \rightarrow O_2 + 4e^- + 4H^+$$
 (2)

## 2.2. XRD and SEM characterization

Ex-situ X-ray diffraction (XRD) measurement was performed using a D8 Advance X-ray Diffractometer (Bruker AXS, Germany) equipped with a Molybdenum radiation source ( $\lambda$  K $\alpha$ <sub>1</sub> = 0.7093 Å) to examine the phase of the deposited copper. Morphology of the surface of the Cu

foils before and after electrodeposition processing, and the foils before and after Li plating/stripping were investigated with using a Scanning Electron Microscope (Hitachi SU8010).

# 2.3. Li plating/stripping tests and cycling performance tests in liquid electrolyte

Standard CR2016-type coin cells were assembled in an Argon (Ar) filled glove box for all liquid-based electrochemical testing, including Li plating/stripping stability tests, Coulombic efficiency tests, electrochemical impedance spectroscopy (EIS), and full-cell cycling tests. For Li plating/stripping and Coulombic efficiency tests, a piece of Li foil with thickness of 0.25 mm was used as the counter electrode, while the electrodeposited Cu foil was used as the working electrode. The electrolyte was 1 M LiTFSI (99.95%, Sigma-Aldrich) in DOL/DME (1,3-Dioxolane, 99%, Sigma-Aldrich/1,2-Dimethoxyethane, 99.5%, Sigma-Aldrich) in 1:1 vol ratio. No additive was used unless otherwise noted. The Li plating/stripping behavior was tested under current density of 2 and 8 mA cm<sup>-2</sup> for 1 and 4 mAh cm<sup>-2</sup>, respectively, in each cycle with using an Arbin BT2043 battery cycler. Bare Cu foils (b-copper) with no deposition and electrodeposited Cu foils with nanometer-sized structure (n-copper) were tested under the same conditions for comparison. In further electrochemical tests, n-copper was used. Columbic efficiency was calculated based on the ratio of Li stripped to Li plated. One wt% LiNO<sub>3</sub> was added into the electrolyte in this test to stabilize the solidelectrolyte-interphase (SEI). The cell was first cycled between 0 and 1 V (versus Li $^+$ /Li) at 50  $\mu A$  for 5 cycles to remove surface contamination and stabilize the SEI. Then,  $1\,\mathrm{mAh\,cm}^{-2}$  of Li was plated onto the Cu current collector under a 1 mA cm<sup>-2</sup> current density, followed with charging to 0.5 V under a current density of 0.5 mA cm<sup>-2</sup>. EIS measurement was conducted using a Bio-Logic MP3 impedance spectrometer in the frequency range of 100 mHz and 100 kHz. For the full-cell tests, LiFePO4 (MTI Corp.) was blended with carbon black (Super P, MTI Corp.) and Polyvinylidene fluoride (PVDF) (Sigma-Aldrich) with a weight ratio of 8:1:1 as the cathode. The cathode film was made using a typical doctor-blade method, with using N-Methyl-2-pyrrolidone (NMP) (J.T. Baker) as the solvent and applying the slurry onto an aluminum foil with an areal capacity of  $\sim 0.73 \, \text{mAh cm}^{-2}$ .  $2 \, \text{mAh cm}^{-2}$  Li was electrochemically deposited onto n-copper to be used as the anode. The full cell was assembled and tested under the rate of 1 C between 2 and 4.2 V. One wt% LiNO<sub>3</sub> was added into the electrolyte. All the reaction and measurements were conducted under room temperature.

#### 2.4. Preparation of solid-state symmetric cells

The solid-state symmetric cells were fabricated as follows: the n/b-copper was used as the working electrode, as-synthesized  $\mathrm{Li_6PS_5Cl}$  (see Supporting information for the process of synthesis) was used as the solid electrolyte, and Li foil was used as counter and reference electrode. The three components were added in order into a polycarbonate tube (12.7 mm inner diameter) and pressed together under a pressure of 50 bar. Finally, the tri-layer assembly was sandwiched between two stainless steel rods which were used as current collectors. The solid state symmetric cells were tested under the same electrochemical parameters as the symmetric coin cells.

#### 2.5. Preparation of solid-state full cells

The solid-state Li@Cu/ Li<sub>6</sub>PS<sub>5</sub>Cl /TiS<sub>2</sub> full cells were fabricated as follows: a composite of TiS<sub>2</sub> and Li<sub>6</sub>PS<sub>5</sub>Cl (9 mg, TiS<sub>2</sub>: Li<sub>6</sub>PS<sub>5</sub>Cl = 1:2 in weight) was used as the cathode, with Li<sub>6</sub>PS<sub>5</sub>Cl (150 mg) as the solid electrolyte, and pre-lithiated Li@Cu as the anode. The anode was pre-lithiated by plating 2 mAh cm $^{-2}$  of Li onto the n-copper foil in a symmetric coin cell and disassembled in the glove box. The tri-layer full cell was set in a polycarbonate tube (1.27 mm in diameter) and pressed together under 50 bar and then sandwiched between two stainless steel

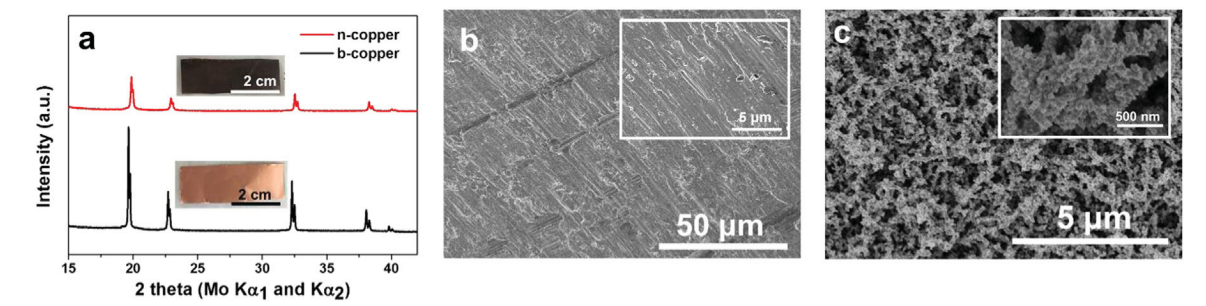


Fig. 1. a) XRD patterns of bare Cu (b-copper) and electrodeposited nanometer-sized Cu (n-copper). Insets are the corresponding photographs of b-copper, and n-copper; b) SEM image of b-copper with a scale bar of  $50 \mu m$ . Inset is the zoom-in view with a scale bar of  $5 \mu m$ ; c) SEM image of n-copper Cu with a scale bar of  $5 \mu m$ . Inset is the zoom-in view with a scale bar of 500 nm.

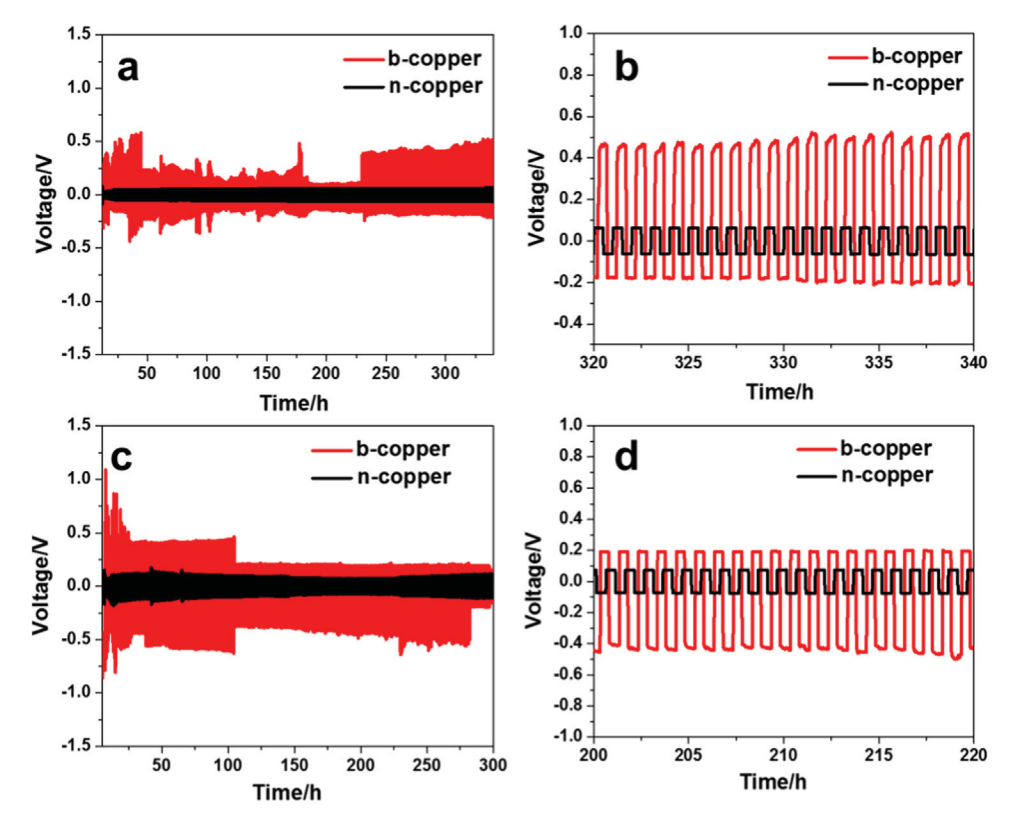


Fig. 2. Voltage profiles of Li plating/stripping of the b-copper and n-copper symmetric cells at a) 1 mAh cm<sup>-2</sup> and c) 4 mAh cm<sup>-2</sup>, respectively. b) The detailed voltage profiles from 320th to 340th cycle in a). d) The detailed voltage profiles from 200th to 220th cycle in c).

current collectors.

#### 3. Results and discussion

# 3.1. Processing and characterization of electrodeposited Cu current collector

To create more nucleation/deposition sites on the surface of the current collector, an electrodeposition process was used to control nanometer-sized structure of Cu on the surface of a conventional copper current collector foil in a 0.5 M copper sulfate heptahydrate solution with PAA-5000 and sulfuric acid as additives. Fig. 1a shows the XRD patterns of the bare and deposited samples and it can be clearly seen that only metallic Cu phase is formed in both electrodeposited films. The insets in Fig. 1a show the photographs of these samples. The nanometer-structured Cu foil sample (hereby denoted as n-copper) shows a dark color, likely due to strong absorption of visible light by the nano-porous film on the surface, unlike the bare copper foil (hereby denoted as b-copper). Fig. 1b and c show the SEM images of b-copper

and n-copper respectively. The n-copper film has a porous 3-D nanostructure consisting of interconnecting primary particles of ~50 nm and the porosity was estimated to be ~76% (see Supporting Information for calculation). Careful analysis of the microstructures indicates that the size of the primary particles, the porosity, and the surface morphology of the porous Cu films can be tuned in a wide range by the type and amount of additives used, which form intermediate complex at the copper substrate and function as seeds to form nanoclusters [46]. The optimal condition of electrodeposition, including the concentration of additives and the deposition time, was determined by a series of tests. Both homogeneity and porosity of the deposited layer are critical for the subsequent electrochemical tests. We expect that the nanometersized primary particles in the n-copper sample can serve as the deposition/nucleation sites for Li plating and the high porosity of the deposited layer may allow more Li storage inside the porous Cu layer, in addition to the Li plated on the top of the Cu layer. It is worth noting that the deposited layers in n-copper are very robust and adhere well to the Cu substrate, implying a good electrical connectivity and good mechanical integrity. The deposited n-copper layer is typically of

 ${\sim}5\,\mu m$  thick and the copper foil is as flexible as previous and can be directly used in roll-to-roll processes.

#### 3.2. Li metal plating/stripping behavior

The performance of the n-copper current collectors in Li platingstripping cycles in various areal capacities was evaluated in symmetric Li/Li@Cu cells using a Li counter/reference electrode and a Cu working electrode, as reported previously [30-40]. For all cells, 2 mAh cm<sup>-2</sup> of Li was first plated onto the electrodeposited Cu current collectors at a constant current density of 2 mA cm<sup>-2</sup>. Then, the symmetric cells were cycled with various areal capacities of 1 and 4 mAh cm<sup>-2</sup>, respectively, with both charge and discharge times of each cycle being set to be 0.5 h (i.e., with current density of 2 and 8 mA cm<sup>-2</sup>, respectively). The voltage profiles are shown in Fig. 2. In the tests of 1 mAh cm<sup>-2</sup>, shown in Fig. 2a, the symmetric cell with b-copper shows spiky voltage oscillations as large as 1 V, implying internal short-circuits, as also reported by others [30-40], likely due to the formation of Li dendrites. In contrast, the n-copper cell shows much better cycling stability with reasonably small voltage amplitude and negligible voltage fluctuations up to 340 h cycling, indicating significantly improved lithium plating/stripping stability. Fig. 2b shows the zoom-in voltage profiles of the three cells within 320-340 h. The voltage amplitude of n-copper is  $\sim 50 \, \text{mV}$ , indicating low interfacial resistance and facilitated ionic and electronic conduction, which can be ascribed to the much larger electroactive surface areas than those of b-copper and a more uniform SEI. The large active surface area of n-copper foil is ascribed not only to the nanostructured top surface, but also the pores in which electrolyte can easily throughout percolate. The resistance to interfacial ionic transport is drastically reduced. In the tests with larger areal capacities of 4 mAh cm<sup>-2</sup> (current density 8 mA cm<sup>-2</sup>), n-copper cells also show excellent stability and far lower resistance than those of the b-copper, as shown in Fig. 2c and d. In commercial Li-ion batteries with graphite or Si-C anode, typical areal capacity ranges from 1.5 to 3 mAh cm<sup>-2</sup> [47,48]. The excellent reversibility and stability in a long time for the n-copper samples at high areal capacities of 4 mAh cm<sup>-2</sup> demonstrates the promise for it to be used in large form cylindrical or pouch cells.

#### 3.3. Morphology evolution of Li deposited on the current collectors

Careful SEM characterizations were used to understand the excellent cycling performance of the electrodeposited copper current collector and to explore the Li storage mechanism. Fig. 3 shows the top view and cross-sectional view of the n-copper foil after Li plating and Li stripping of various capacities, respectively. In Fig. 3a, the size of the primary particles obviously increases from ~50 nm in pristine film (Fig. 1c) to  $\sim$ 200 nm after 1 mAh cm<sup>-2</sup> plating, indicating substantial amount of Li is plated onto the surface of Cu particles. Meanwhile, the porosity of the surface layer visually decreases significantly, implying that Li is also deposited into the pores. For comparison, images of bcopper are also provided in Fig. S1, from which large amount of Li dendrites form on top of b-copper can be seen. With increasing amount of Li plated to 2 and 4 mAh cm<sup>-2</sup>, it can be clearly seen that the size of the primary particles further increases to  $\sim$ 400 nm (2 mAh cm<sup>-2</sup>), and eventually, ~800 nm (4 mAh cm<sup>-2</sup>), yet still with a smooth and granular surface, as shown in Fig. 3b and c. When the capacity increases to 6 mAh cm<sup>-2</sup>, as shown in Fig. 3d, the individual particles are large enough to interconnect and form locally flat surfaces where island-like Li dendrites can grow from, same as what commonly occurs on the surface of Li foil. The suppression of Li dendrite growth is due to the direct deposition only on the highly conductive Cu both on top surface and into the pores, but not on the flat surface of Li.

For Li metal anode, it is confusing to use "theoretical capacity" as the capacity limit, as the maximum amount of Li deposition that would not stimulate dendrites growth oftentimes is not a clear cut. Therefore, we suggest using "practical capacity" to refer to the capacity limit. In this case, the practical areal capacity of n-copper sample processed with current electrodeposition parameters seems to be between 4 and 6 mAh cm<sup>-2</sup>. This capacity is higher than the maximum amount of Li that can be stored in the pores (see Supporting information for calculation) of the 3-D structure, indicating the structure itself could effectively reduce local current density and accommodate more homogeneous Li deposition on top of the structure. However, this value already exceeds that of commercial graphite anodes and can be further improved with increasing the thickness and porosity and tuning the morphology and composition of the deposition layer.

In the Li stripping tests with capacities of 1, 2, 4, and 6 mAh cm<sup>-2</sup>, the current densities were set at 2, 4, 8, and 12 mA cm<sup>-2</sup>, as shown in Fig. 3e, f, g, and h, respectively. It is shown that for the tests of 1, 2, and 4 mAh cm<sup>-2</sup>, after stripping, the granular morphology of n-copper is retained, yet with decreased porosity and increased size of primary particles, which is mainly due to the remaining SEI covering on the surface of Cu particles. However, after 6 mAh cm<sup>-2</sup> deposition, as shown in Fig. 3h, the stripping of same capacity results in a very different morphology, with irregular matrix of connecting large particles and some voids.

From the cross-sectional view of Li plating/stripping in Fig. 3(i-l), there is a clear trend that with increasing plating capacity, the primary particle size increases throughout the whole thickness of the porous layer yet with little Li dendrite grown on top of the surface, confirming the Li storage in the pores and preferably deposit on Cu nanoparticle sites due to the lower local current density. Compared with bare Cu, the n-copper offers more nucleation sites for Li to avoid dendrite formation. With the proceeding of Li stripping, the pristine porous structure can be largely retained, comparing with cross-sectional view image of pristine n-copper (Fig. S2). In both plating and stripping processes, the thickness of the electrodeposited Cu layer does not change significantly, implying the Li deposition pathway is good for maintaining a more homogeneous morphology thus relatively constant volume of the anode during cycling. Fig. 3m schematically shows the Li storage mechanism with increasing deposition capacities. When the deposition capacity is small, the storage in the pores is the major mechanism; while when the deposition capacity is large, the deposition on the top is the major storage mechanism. Even after all top surface is covered by deposited Li, because the top surface still has nanometer sized features and still offers many nucleation sites. The deposition of Li on the top surface is still reasonably homogeneous and with no dendrites, until the plating capacity is too large (in this case, ~6 mAh/cm<sup>2</sup>) and the deposited Li largely flattens the top surface.

## 3.4. Electrochemical characterization and testing

Electrochemical cycling tests on symmetric cells with constantcurrent plating (cut with designed capacities) and constant-current stripping (cut with 0.5 V voltage limit) were done and the results are shown Supporting information (Fig. S3). To evaluate the feasibility of using this electrodeposited Cu in practical battery systems, full-cell tests were performed. Both n-copper and b-copper were first pre-lithiated in a symmetric cell with 2 mAh cm<sup>-2</sup> of Li. Then the symmetric cell was taken apart and the obtained lithiated n-copper and b-copper were used as the anode coupled with a LiFePO<sub>4</sub> cathode. Fig. 4a shows the voltage-capacity profiles of the cells with b-copper and n-copper anodes at  $0.1 \text{ C} (1 \text{ C} = 170 \text{ mA g}^{-1})$  in a voltage window of 2.0–4.2 V. The cycling up to 4.2 V may induce some minor gradual loss of the ether-based electrolyte, but this did not seem to significantly affect the cycling performance up to 100 cycles. The cell with n-copper anode delivers an initial discharge capacity of 154.6 mAh g<sup>-1</sup>, slightly higher than 149.5 mAh g<sup>-1</sup> for the b-copper cell. Fig. 4b presents the charge/discharge curves of the cell with n-copper substrate in the 1st, 2nd, and 10th charge/discharge cycles at 0.1 C, showing good consistency of the voltage profile. In the higher rate cycling tests at 1 C (Fig. 4c), the cell with b-copper anode presents a capacity decay from 132.6 to

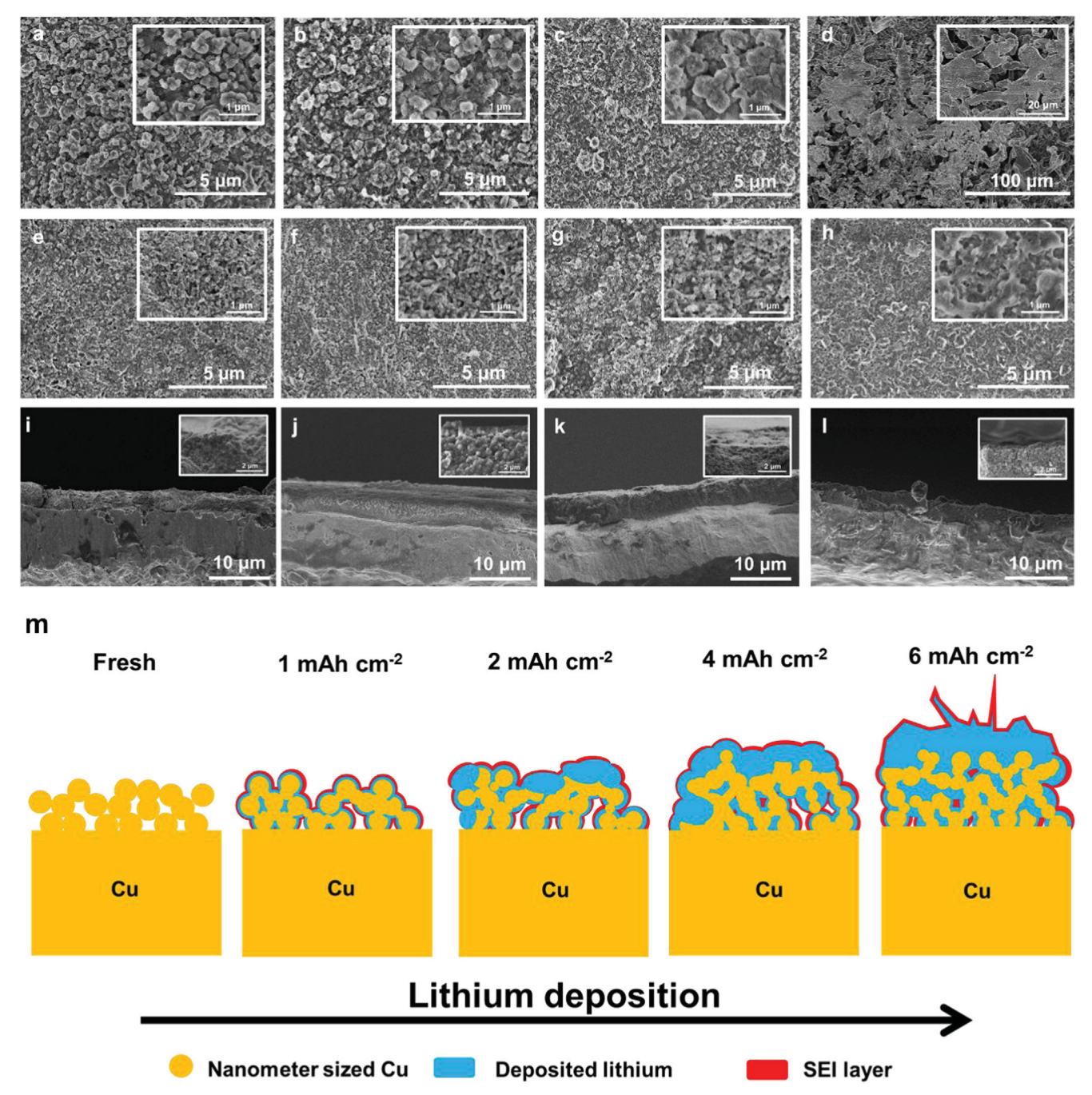


Fig. 3. Morphology of deposited Li metal characterized by SEM. Top view images of n-copper electrode after Li plating of a)  $1 \text{ mAh cm}^{-2}$ , b)  $2 \text{ mAh cm}^{-2}$ , c)  $4 \text{ mAh cm}^{-2}$ , and d)  $6 \text{ mAh cm}^{-2}$ . Top view images of n-copper electrode after Li stripping of e)  $1 \text{ mAh cm}^{-2}$ , f)  $2 \text{ mAh cm}^{-2}$ , g)  $4 \text{ mAh cm}^{-2}$ , and h)  $6 \text{ mAh cm}^{-2}$ . Scale bars are  $5 \text{ \mu m}$ . Insets are the zoom-in view with scale bars of  $1 \text{ \mu m}$ ; Cross-sectional SEM images of n-copper electrode after i)  $1 \text{ mAh cm}^{-2}$  and j)  $4 \text{ mAh cm}^{-2}$  of Li plating. Scale bars are  $10 \text{ \mu m}$ . Insets are the zoom-in views with scale bars of  $2 \text{ \mu m}$ ; Cross-sectional SEM images of n-copper after Li stripping of k)  $1 \text{ mAh cm}^{-2}$  and l)  $4 \text{ mAh cm}^{-2}$ . Scale bars are  $10 \text{ \mu m}$ . Insets are the zoom-in views with scale bars of  $2 \text{ \mu m}$ . The yellow dotted lines denote the boundaries between n-copper (top) and Cu substrate (bottom); m) Schematic illustration of n-copper current collector deposited with various amount of Li.

92.6 mAh g<sup>-1</sup> in 100 cycles with a capacity retention of 69.8%. In comparison, the cell with n-copper anode exhibits excellent cycling performance. It delivers a capacity of 127.6 mAh g<sup>-1</sup> after 100 cycles and with a capacity retention of 95%. The Coulombic efficiency of the cell with electrodeposited n-copper anode is ~99.66% at 1 C upon 100 cycles, which is much better than that with b-copper substrate and is comparable to high performance carbonaceous-based current collector material [36,39,40]. Though comparable with the reported work, the capacity fading of the liquid full-cell is slightly faster than that of conventional half cells with LiFePO<sub>4</sub> cathode. This is possibly due to

that our anode has much less Li than Li foil used in half cells and the irreversible Li consumption resulted from SEI formation and clogged pores. In short, the electrochemical performance of n-copper used in the LiFePO $_4$  full cell shows its potential in practical application. A lager form  $5\,\mathrm{cm}\,^*5\,\mathrm{cm}$  single layer pouch cell was also assemble and tested. The performance is similar to what was obtained in coin cells (see Fig. S4 in Supplement information), which further demonstrates the scalability of this method.

To explore the possibility of using this novel 3-D nanostructured current collector in all-solid-state batteries, which is another promising

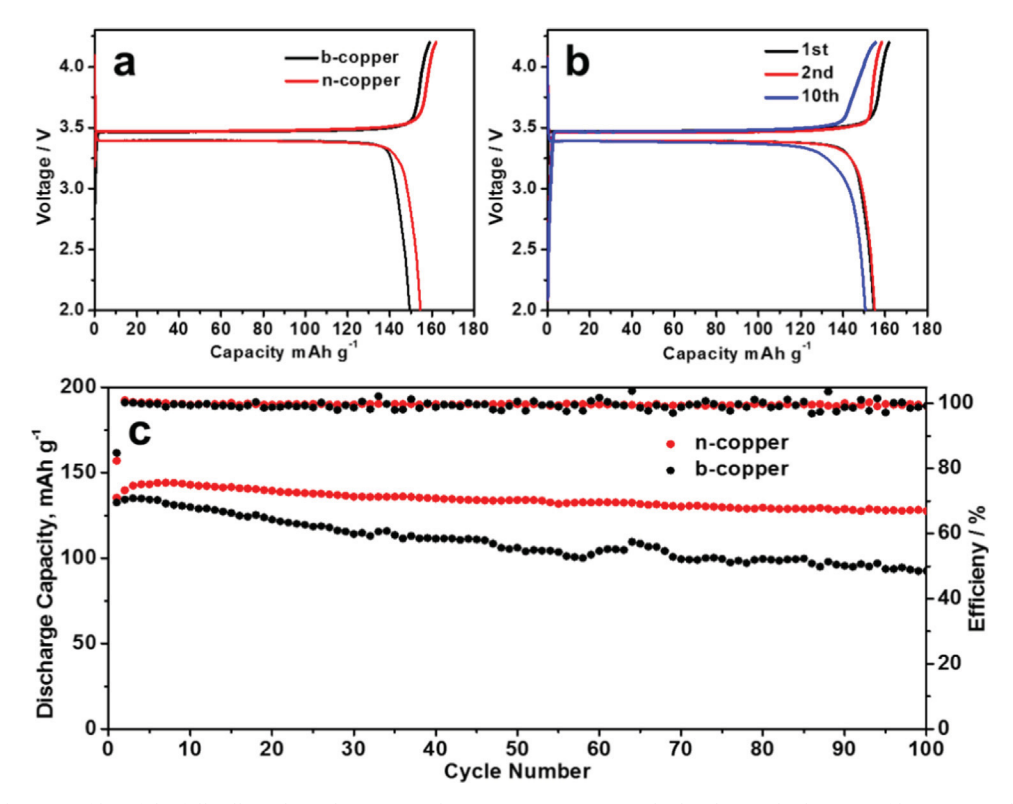


Fig. 4. a) Charge/discharge profiles of the full cells with Li@b-copper and Li@n-copper, respectively. b) Charge/discharge profiles at 1st, 2nd, and 10th cycle of the full cell with Li@n-copper electrode. c) Cycling performance and CE of full cells with Li@b-copper and Li@n-copper at 1 C.

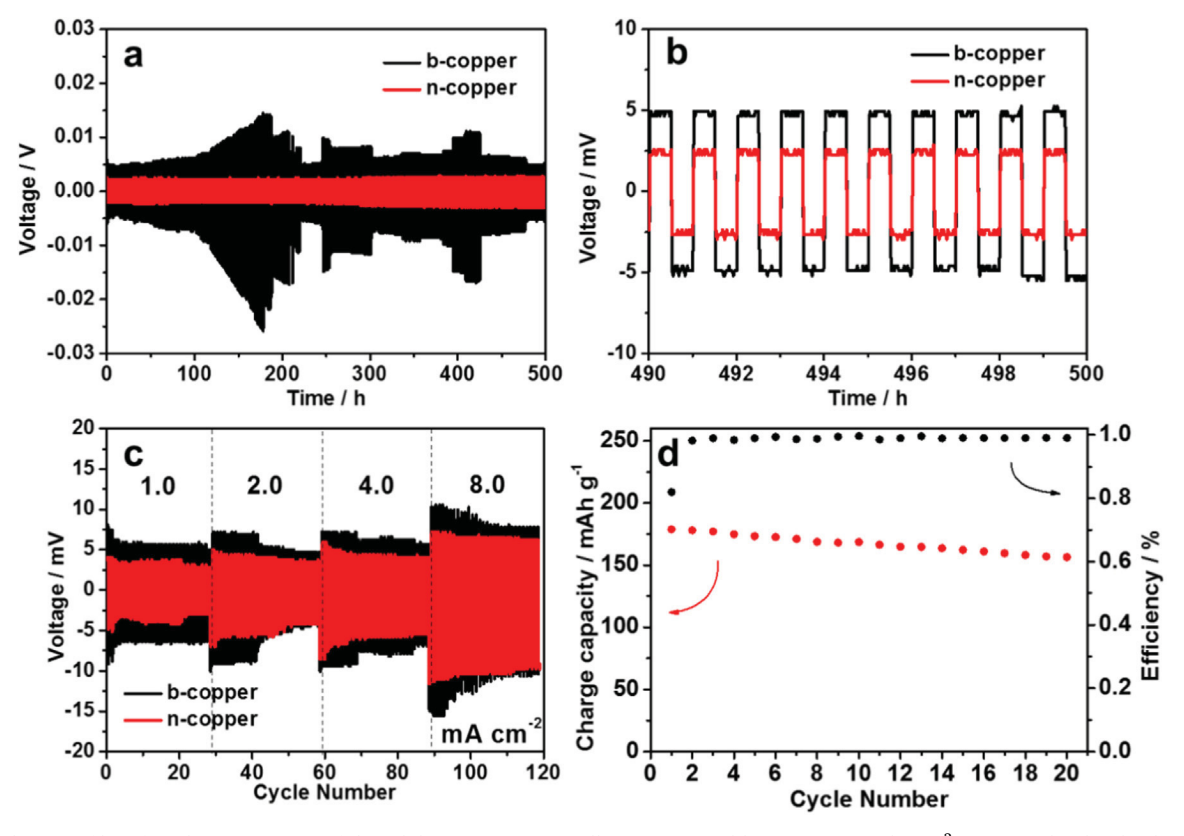


Fig. 5. a) Voltage profiles of Li plating/stripping of the solid state symmetric cells (n-copper at 1 mAh cm $^{-2}$ , respectively); b) The detailed voltage profiles from 490th–500th cycle in (a); c) Rate performance of Li plating/stripping of the solid-state symmetric cells (n-copper and b-copper at various current densities); d) Cycling performance of the solid-state Li@n-copper/TiS $_2$  full cells at 0.2 C.

technology that requires usage of Li-metal anodes, tests were conducted in both symmetric and full cells. The symmetric cells (Li/Li@Cu) used Li<sub>6</sub>PS<sub>5</sub>Cl (XRD pattern of as-synthesized Li<sub>6</sub>PS<sub>5</sub>Cl is shown in Fig. S5) as electrolyte, Li foil as counter electrode, and b-copper or n-copper as working electrode. As shown in Fig. 5a, cell with b-copper shows larger voltage fluctuations, while for the cell with n-copper, excellent cycling stability as well as much smaller voltage hysteresis is observed and the performance stays unchanged for more than 500 h (Fig. 5b), indicating good interface compatibility and stable plating/stripping at the solidsolid interface as well. Cycling tests at various current densities were also conducted to evaluate the rate performance. It is obvious that cell with n-copper current collector exhibits smaller voltage fluctuations than that of b-copper upon different areal densities (Fig. 5c). An allsolid-state full cell was also assembled with using pre-lithiated n-copper as anode and TiS2 as cathode to explore the potential of applications in all-solid-state batteries. Fig. S6 shows the cross-sectional view of the assembled all-solid-state battery. As shown in Fig. S7, the solid-state full cell shows the typical charge and discharge curve of TiS2, which is in consistent with previous reports [49]. As shown in Fig. 5d, solid-state cell with n-copper can deliver an initial reversible capacity of  $179 \text{ mAh g}^{-1}$  at 0.2 C (1 C =  $239 \text{ mA g}^{-1}$ ) at  $20 \,^{\circ}$ C. After 20 cycles, it can still maintain a reversible capacity of 156.5 mAh g<sup>-1</sup> with a CE of 99.3%, corresponding to the capacity retention of 87.5%. This result demonstrates the possible practical application of the electrodeposited n-copper current collector in all-solid-state battery systems.

#### 4. Conclusion

In conclusion, we have demonstrated the capability of electrodeposited Cu 3-D nanostructures of accommodating Li within its porous structure and on the top surface, which effectively suppresses Li dendrite formation and provides a very high practical Li storage areal capacity of  $> 4 \,\mathrm{mAh}\,\mathrm{cm}^{-2}$ . The full cell tests with using both liquid electrolyte and solid electrolyte show exciting high performances. Most importantly, this facile one-step electrodeposition method is very scalable for mass production. One easy configuration to realize it in industrial scale is schematically shown in Fig. S8. The 3-D structure of Cu can be simultaneously deposited on both sides of standard Cu foils for bi-polar designs. The nanoporous layered electrodeposition coated Cu foil can be produced with very low cost and this foil can be seamlessly incorporated into current Li-ion battery production lines with no major changes required. In addition, this current collector can be used not only in Li-ion, but also in Li-S and Li-O2 batteries, providing cathode problems solved. The electrodeposition method also provides a lot of flexibility and tunability of the deposited structure, which suggests more Li may be accommodated and ultrahigh energy density batteries may be developed along this promising approach.

#### Acknowledgements

X.M., Z.L., and H.C. acknowledge funding support from Georgia Institute of Technology, and the National Science Foundation of the U.S. under grant numbers CBET1605692 and CBET1706723.

## Appendix A. Supporting information

Supplementary data associated with this article can be found in the online version at doi:10.1016/j.nanoen.2019.02.048.

#### References

- M.K. Song, E.J. Cairns, Y. Zhang, Lithium/sulfur batteries with high specific energy: old challenges and new opportunities, Nanoscale 5 (2013) 2186, https://doi.org/ 10.1039/c2nr33044i.
- [2] P.G. Bruce, S.A. Freunberger, L.J. Hardwick, J.M. Tarascon, Li–O2 and Li–S batteries with high energy storage, Nat. Mater. 11 (2012) 19–29, https://doi.org/10.1038/nmat3191.

[3] A. Manthiram, X. Yu, S. Wang, Lithium battery chemistries enabled by solid-state electrolytes, Nat. Rev. Mater. 2 (2017) 1–16, https://doi.org/10.1038/natrevmats. 2016.103.

- [4] J.C. Bachman, S. Muy, A. Grimaud, H.H. Chang, N. Pour, S.F. Lux, O. Paschos, F. Maglia, S. Lupart, P. Lamp, L. Giordano, Y. Shao-Horn, Inorganic solid-state electrolytes for lithium batteries: mechanisms and properties governing ion conduction, Chem. Rev. 116 (2016) 140–162, https://doi.org/10.1021/acs.chemrev. 5b00563.
- [5] W. Xu, J. Wang, F. Ding, X. Chen, E. Nasybulin, Y. Zhang, J.-G. Zhang, Lithium metal anodes for rechargeable batteries, Energy Environ. Sci. 7 (2012) 513–537, https://doi.org/10.1039/C3EE40795K.
- [6] A. Zhamu, G. Chen, C. Liu, D. Neff, Q. Fang, Z. Yu, W. Xiong, Y. Wang, X. Wang, B.Z. Jang, Reviving rechargeable lithium metal batteries: enabling next-generation high-energy and high-power cells, Energy Environ. Sci. 5 (2012) 5701–5707, https://doi.org/10.1039/C2FE02911A.
- [7] K.J. Harry, D.T. Hallinan, D.Y. Parkinson, A.A. MacDowell, N.P. Balsara, Detection of subsurface structures underneath dendrites formed on cycled lithium metal electrodes, Nat. Mater. 13 (2014) 69–73, https://doi.org/10.1038/nmat3793.
- [8] D. Lv, Y. Shao, T. Lozano, W.D. Bennett, G.L. Graff, B. Polzin, J. Zhang, M.H. Engelhard, N.T. Saenz, W.A. Henderson, P. Bhattacharya, J. Liu, J. Xiao, Failure mechanism for fast-charged lithium metal batteries with liquid electrolytes, Adv. Energy Mater. 5 (2015) 1–7, https://doi.org/10.1002/aenm.201400993.
- [9] Y. Sun, N. Liu, Y. Cui, Promises and challenges of nanomaterials for lithium-based rechargeable batteries, Nat. Energy 1 (2016) 1–12, https://doi.org/10.1038/ nenergy 2016 71
- [10] E. Peled, The electrochemical behavior of alkali and alkaline earth metals in non-aqueous battery systems—the solid electrolyte interphase model, J. Electrochem. Soc. 126 (1979) 2047, https://doi.org/10.1149/1.2128859.
- [11] M. Arakawa, S. ichi Tobishima, Y. Nemoto, M. Ichimura, J. ichi Yamaki, Lithium electrode cycleability and morphology dependence on current density, J. Power Sources 43 (1993) 27–35, https://doi.org/10.1016/0378-7753(93)80099-B.
- [12] C. Brissot, M. Rosso, J.N. Chazalviel, S. Lascaud, Dendritic growth mechanisms in lithium/polymer cells, J. Power Sources 81 (1999) 925–929, https://doi.org/10. 1016/S0378-7753(98)00242-0.
- [13] M. Rosso, T. Gobron, C. Brissot, J.N. Chazalviel, S. Lascaud, Onset of dendritic growth in lithium/polymer cells, J. Power Sources 97–98 (2001) 804–806, https:// doi.org/10.1016/S0378-7753(01)00734-0.
- [14] K. Kanamura, Electrochemical deposition of very smooth lithium using nonaqueous electrolytes containing HF, J. Electrochem. Soc. 143 (1996) 2187, https://doi.org/ 10.1149/1.1836979.
- [15] Y. Lu, Z. Tu, L.A. Archer, Stable lithium electrodeposition in liquid and nanoporous solid electrolytes, Nat. Mater. 13 (2014) 961–969, https://doi.org/10.1038/ nmat4041.
- [16] J. Guo, Z. Wen, M. Wu, J. Jin, Y. Liu, Vinylene carbonate-LiNO3: a hybrid additive in carbonic ester electrolytes for SEI modification on Li metal anode, Electrochem. Commun. 51 (2015) 59–63. https://doi.org/10.1016/j.elecom.2014.12.008.
- [17] W. Li, H. Yao, K. Yan, G. Zheng, Z. Liang, Y.M. Chiang, Y. Cui, The synergetic effect of lithium polysulfide and lithium nitrate to prevent lithium dendrite growth, Nat. Commun. 6 (2015) 1–8, https://doi.org/10.1038/ncomms8436.
- [18] H. Ye, Y.X. Yin, S.F. Zhang, Y. Shi, L. Liu, X.X. Zeng, R. Wen, Y.G. Guo, L.J. Wan, Synergism of Al-containing solid electrolyte interphase layer and Al-based colloidal particles for stable lithium anode, Nano Energy 36 (2017) 411–417, https://doi. org/10.1016/j.nanoen.2017.04.056.
- [19] K. Yan, H.W. Lee, T. Gao, G. Zheng, H. Yao, H. Wang, Z. Lu, Y. Zhou, Z. Liang, Z. Liu, S. Chu, Y. Cui, Ultrathin two-dimensional atomic crystals as stable interfacial layer for improvement of lithium metal anode, Nano Lett. 14 (2014) 6016–6022, https://doi.org/10.1021/nl503125u.
- [20] G. Zheng, S.W. Lee, Z. Liang, H.W. Lee, K. Yan, H. Yao, H. Wang, W. Li, S. Chu, Y. Cui, Interconnected hollow carbon nanospheres for stable lithium metal anodes, Nat. Nanotechnol. 9 (2014) 618–623, https://doi.org/10.1038/nnano.2014.152.
- [21] C. Huang, J. Xiao, Y. Shao, J. Zheng, W.D. Bennett, D. Lu, L.V. Saraf, M. Engelhard, L. Ji, J. Zhang, X. Li, G.L. Graff, J. Liu, Manipulating surface reactions in lithiumsulphur batteries using hybrid anode structures, Nat. Commun. 5 (2014) 1–7, https://doi.org/10.1038/ncomms4015.
- [22] Q. Pang, X. Liang, A. Shyamsunder, L.F. Nazar, An in vivo formed solid electrolyte surface layer enables stable plating of Li metal, Joule 1 (2017) 871–886, https:// doi.org/10.1016/j.joule.2017.11.009.
- [23] N.W. Li, Y. Shi, Y.X. Yin, X.X. Zeng, J.Y. Li, C.J. Li, L.J. Wan, R. Wen, Y.G. Guo, A flexible solid electrolyte interphase layer for long-life lithium metal anodes, Angew. Chem. Int. Ed. 57 (2018) 1505–1509, https://doi.org/10.1002/anie.201710806.
- [24] H. Duan, Y.X. Yin, Y. Shi, P.F. Wang, X.D. Zhang, C.P. Yang, J.L. Shi, R. Wen, Y.G. Guo, L.J. Wan, Dendrite-free Li-metal battery enabled by a thin asymmetric solid electrolyte with engineered layers, J. Am. Chem. Soc. 140 (2018) 82–85, https://doi.org/10.1021/jacs.7b10864.
- [25] X. Cheng, C. Yan, X. Cheng, C. Yan, X. Chen, C. Guan, J. Huang, H. Peng, implantable solid electrolyte interphase in lithium-metal batteries implantable solid electrolyte interphase in lithium-metal batteries, Chempr 2 (2017) 258–270, https://doi.org/10.1016/j.chempr.2017.01.003.
- [26] D. Wang, W. Zhang, W. Zheng, X. Cui, T. Rojo, Q. Zhang, Towards high-safe lithium metal anodes: suppressing lithium dendrites via tuning surface energy, Adv. Sci. 4 (2017), https://doi.org/10.1002/advs.201600168.
- [27] S. Choudhury, R. Mangal, A. Agrawal, L.A. Archer, A highly reversible room-temperature lithium metal battery based on crosslinked hairy nanoparticles, Nat. Commun. 6 (2015) 1–9, https://doi.org/10.1038/ncomms10101.
- [28] X. Han, Y. Gong, K. Fu, X. He, G.T. Hitz, J. Dai, A. Pearse, B. Liu, H. Wang, G. Rubloff, Y. Mo, V. Thangadurai, E.D. Wachsman, L. Hu, Negating interfacial

impedance in garnet-based solid-state Li metal batteries, Nat. Mater. 16 (2017) 572–579, https://doi.org/10.1038/nmat4821.

- [29] X.X. Zeng, Y.X. Yin, N.W. Li, W.C. Du, Y.G. Guo, L.J. Wan, Reshaping lithium plating/stripping behavior via bifunctional polymer electrolyte for room-temperature solid Li metal batteries, J. Am. Chem. Soc. 138 (2016) 15825–15828, https:// doi.org/10.1021/jacs.6b10088.
- [30] C.P. Yang, Y.X. Yin, S.F. Zhang, N.W. Li, Y.G. Guo, Accommodating lithium into 3D current collectors with a submicron skeleton towards long-life lithium metal anodes, Nat. Commun. 6 (2015) 1–9, https://doi.org/10.1038/ncomms9058.
- [31] L.L. Lu, J. Ge, J.N. Yang, S.M. Chen, H. Bin Yao, F. Zhou, S.H. Yu, Free-standing copper nanowire network current collector for improving lithium anode performance, Nano Lett. 16 (2016) 4431–4437, https://doi.org/10.1021/acs.nanolett. 6b01581.
- [32] L. Liu, Y.X. Yin, J.Y. Li, N.W. Li, X.X. Zeng, H. Ye, Y.G. Guo, L.J. Wan, Free-standing hollow carbon fibers as high-capacity containers for stable lithium metal anodes, Joule 1 (2017) 563–575, https://doi.org/10.1016/j.joule.2017.06.004.
- [33] T.T. Zuo, X.W. Wu, C.P. Yang, Y.X. Yin, H. Ye, N.W. Li, Y.G. Guo, Graphitized carbon fibers as multifunctional 3D current collectors for high areal capacity Li anodes, Adv. Mater. 29 (2017) 1–6, https://doi.org/10.1002/adma.201700389.
- [34] Q. Yun, Y.B. He, W. Lv, Y. Zhao, B. Li, F. Kang, Q.H. Yang, Chemical dealloying derived 3D Porous current collector for Li metal anodes, Adv. Mater. 28 (2016) 6932–6939, https://doi.org/10.1002/adma.201601409.
- [35] S.H. Wang, Y.X. Yin, T.T. Zuo, W. Dong, J.Y. Li, J.L. Shi, C.H. Zhang, N.W. Li, C.J. Li, Y.G. Guo, Stable Li metal anodes via regulating lithium plating/stripping in vertically aligned microchannels, Adv. Mater. 29 (2017) 1–8, https://doi.org/10. 1002/adma.201703729.
- [36] S. Liu, A. Wang, Q. Li, J. Wu, K. Chiou, J. Huang, J. Luo, Crumpled graphene balls stabilized dendrite-free lithium metal anodes, Joule 2 (2017) 184–193, https://doi. org/10.1016/j.joule.2017.11.004.
- [37] K. Yan, B. Sun, P. Munroe, G. Wang, Three-dimensional pie-like current collectors for dendrite-free lithium metal anodes, Energy Storage Mater. 11 (2018) 127–133, https://doi.org/10.1016/j.ensm.2017.10.012.
- [38] A. Zhang, X. Fang, C. Shen, Y. Liu, C. Zhou, A carbon nanofiber network for stable lithium metal anodes with high Coulombic efficiency and long cycle life, Nano Res. 9 (2016) 3428–3436, https://doi.org/10.1007/s12274-016-1219-2.
- [39] R. Zhang, X.R. Chen, X. Chen, X.B. Cheng, X.Q. Zhang, C. Yan, Q. Zhang, Lithiophilic sites in doped graphene guide uniform lithium nucleation for dendritefree lithium metal anodes, Angew. Chem. Int. Ed. 56 (2017) 7764–7768, https:// doi.org/10.1002/anie.201702099.
- [40] L. Liu, Y.-X. Yin, J.-Y. Li, S.-H. Wang, Y.-G. Guo, L.-J. Wan, Uniform lithium nucleation/growth induced by lightweight nitrogen-doped graphitic carbon foams for high-performance lithium metal anodes, Adv. Mater. (2018) 1706216, https://doi.org/10.1002/adma.201706216.
- [41] K. Yan, Z. Lu, H.-W. Lee, F. Xiong, P.-C. Hsu, Y. Li, J. Zhao, S. Chu, Y. Cui, Selective deposition and stable encapsulation of lithium through heterogeneous seeded growth. Nat. Energy 1 (2016) 16010. https://doi.org/10.1038/nenergy.2016.10.
- [42] X. Liang, Q. Pang, I.R. Kochetkov, M.S. Sempere, H. Huang, X. Sun, L.F. Nazar, A facile surface chemistry route to a stabilized lithium metal anode, Nat. Energy 2 (2017) 17119, https://doi.org/10.1038/nenergy.2017.119.
- [43] X.B. Cheng, T.Z. Hou, R. Zhang, H.J. Peng, C.Z. Zhao, J.Q. Huang, Q. Zhang, Dendrite-free lithium deposition induced by uniformly distributed lithium ions for efficient lithium metal batteries, Adv. Mater. 28 (2016) 2888–2895, https://doi. org/10.1002/adma.201506124.
- [44] B. Zhu, Y. Jin, X. Hu, Q. Zheng, S. Zhang, Q. Wang, J. Zhu, Poly(dimethylsiloxane) thin film as a stable interfacial layer for high-performance lithium-metal battery anodes, Adv. Mater. 29 (2017) 2–7, https://doi.org/10.1002/adma.201603755.
- [45] N.D. Nikolić, K.I. Popov, L.J. Pavlović, M.G. Pavlović, Morphologies of copper deposits obtained by the electrodeposition at high overpotentials, Surf. Coat. Technol. 201 (2006) 560–566, https://doi.org/10.1016/j.surfcoat.2005.12.004.
- [46] S. Arai, T. Kitamura, Simple method for fabrication of three-dimensional (3D)

- copper nanostructured architecture by electrodeposition, ECS Electrochem. Lett. 3 (2014) D7–D9, https://doi.org/10.1149/2.004405eel.
- [47] N. Nitta, G. Yushin, High-capacity anode materials for lithium-ion batteries: choice of elements and structures for active particles, Part. Part. Syst. Charact. 31 (2014) 317–336, https://doi.org/10.1002/ppsc.201300231.
- [48] M. Ko, S. Chae, J. Ma, N. Kim, H.W. Lee, Y. Cui, J. Cho, Scalable synthesis of siliconnanolayer-embedded graphite for high-energy lithium-ion batteries, Nat. Energy 1 (2016) 1–8, https://doi.org/10.1038/nenergy.2016.113.
- [49] B.R. Shin, Y.J. Nam, D.Y. Oh, D.H. Kim, J.W. Kim, Y.S. Jung, Comparative study of TiS2/Li-In all-solid-state lithium batteries using glass-ceramic Li3PS4and Li10GeP2S12 solid electrolytes, Electrochim. Acta 146 (2014) 395–402, https://doi.org/10.1016/j.electacta.2014.08.139.



**Xuetian Ma** is currently a Ph.D. student in Dr. Hailong Chen's group at Georgia Institute of Technology. Prior to that, she received her M.S. degree and B.S. degree from Cornell University (2014) and Tsinghua University (2012) with a major in Materials Science and Engineering, respectively. Her Ph.D. research focuses on understanding formation of metals and alloys in solution with in situ characterizations.



Zhantao Liu received his B.S. degree (2011) in Beijing University of Aeronautics and Astronautics and M. S. degree (2014) in Hong Kong University of Science and Technology. He is currently a Ph.D. student in Dr. Hailong Chen's group at Georgia Institute of Technology. His research mainly focuses on solid state electrolytes and solid state batteries.



Hailong Chen is an Assistant Professor of the Woodruff School of Mechanical Engineering at Georgia Institute of Technology. He received his B.S. and M.S. from Tsinghua University and Ph.D. from Stony Brook University. His research interests include design of novel electrode materials for Li-ion and Na-ion batteries and solid state electrolytes with using combined computational and experimental approaches. His research also focuses on development of in situ X-ray structural characterization techniques.